Electrochimica Acta 54 (2009) 7099–7105

Contents lists available at ScienceDirect

Electrochimica Acta

journal homepage: www.elsevier.com/locate/electacta

Investigation of fuel and media flexible laminar flow-based fuel cells

Fikile R. Brushett[1], Ranga S. Jayashree[1,2], Wei-Ping Zhou[3], Paul J.A. Kenis*

Department of Chemical & Biomolecular Engineering, University of Illinois at Urbana Champaign, 600 S. Mathews Avenue, Urbana, IL 61801, USA

ARTICLE INFO

Article history:
Received 21 May 2009
Received in revised form 25 June 2009
Accepted 7 July 2009
Available online 15 July 2009

Keywords:
LFFC
Membraneless fuel cell
Laminar flow
Anode characterization
Hydrogen cathode

ABSTRACT

We investigate the performance of air-breathing laminar flow-based fuel cells (LFFCs) operated with five different fuels (formic acid, methanol, ethanol, hydrazine, and sodium borohydride) in either acidic or alkaline media. The membraneless LFFC architecture enables interchangeable operation with different fuel and media combinations that are only limited by the actual anode catalyst used. Furthermore, operating under alkaline conditions significantly improves methanol and ethanol oxidation kinetics and stabilizes sodium borohydride. LFFCs operated with hydrazine and sodium borohydride as fuels exhibit power densities of 80 and 101 mW/cm^2, respectively. To optimize anode performance, particularly for ethanol electro-oxidation, we introduced a hydrogen cathode to the membraneless LFFC design which renders the cell an ideal platform for anode investigation. Here, we highlight two simple diagnostic methods, *in situ* single electrode studies and electrochemical impedance spectroscopy (EIS), for characterizing and optimizing the performance of a direct ethanol LFFC anode.

1. Introduction

A continuously growing need for miniaturized power sources for portable electronic applications has promoted the development of many novel micro-scale fuel cells [1,2]. Compared to conventional batteries, fuel cells offer higher efficiencies and higher energy densities. Furthermore, unlike batteries, fuel cells may be instantaneously recharged by replacing fuel cartridges. Hydrogen fueled polymer electrolyte membrane fuel cells (PEMFCs) are among the most developed fuel cell technologies and are used for low-temperature stationary and extraterrestrial applications [3]. However, for portable applications, safety concerns and practical issues associated with on-board hydrogen storage have spurred research towards the development of direct liquid fuel cells that benefit from the high energy density and easier storage of many organic fuels. Nafion (acidic) membrane-based direct methanol fuel cells (DMFCs) and direct formic acid fuel cells (DFAFCs) have been the most extensively researched for portable applications [4,5]. Traditionally, direct liquid alkaline membrane fuel cell technologies have been hampered by carbonate formation which clogs membrane pores and deactivates electrocatalysts. Recently, significant efforts have been focused on developing high performance anion exchange membranes (AEMs) for alkaline fuel cells which reduce the adverse effects of carbonate formation [6–8]. Despite these improvements, the performance of both alkaline and acidic membrane-based fuel cells is hindered by membrane-related issues such as water management (*i.e.* electrode dry-out/flooding) and fuel crossover. The former occurs at higher current densities when the water generated or consumed at the respective electrodes cannot be removed or replenished sufficiently quickly to maintain stable performance. Thus, such membrane-based systems at times require ancillary components, *i.e.* water management systems, which increase device complexity and lower the overall specific energy of the system. The second, fuel crossover, occurs when fuel migrates through the membrane and reacts on the cathode causing mixed potentials, thereby reducing performance. Crossover may be mitigated by diluting fuel streams but this, in turn, reduces system energy density.

To overcome these membrane-related issues, we have developed air-breathing laminar flow-based fuel cells (LFFCs) where fuel and electrolyte streams are compartmentalized in a single microchannel allowing for ionic transport and eliminating the need for a physical barrier (Fig. 1) [9,10]. A gas diffusion electrode (GDE) exposed to ambient air is used as the cathode [11]. The simple membraneless architecture eliminates water management issues, facilitates by-product removal (*i.e.* carbonates) and enables fuel and media flexibility. Moreover, on the micro-scale, fuel crossover can only occur via diffusion (laminar flow regime) and may be minimized by adjusting stream flow rates and varying channel dimensions [12]. Placing a reference electrode at the fuel cell outlet allows for independent analysis of individual

* Corresponding author at: RAL 115, MC-712 Box C-3, 600 S. Mathews Ave, Urbana, IL 61801, USA. Tel.: +1 217 265 0523; fax: +1 217 333 5052.
E-mail address: kenis@illinois.edu (P.J.A. Kenis).
[1] These authors contributed equally to this work.
[2] Present address: P.O. Box 4098, Chemistry Department, Georgia State University, Atlanta, GA 30302, USA.
[3] Present address: Bldg. 55, Brookhaven Ave., Brookhaven National Lab, Upton, NY 11973, USA.

0013-4686/$ – see front matter © 2009 Elsevier Ltd. All rights reserved.
doi:10.1016/j.electacta.2009.07.011

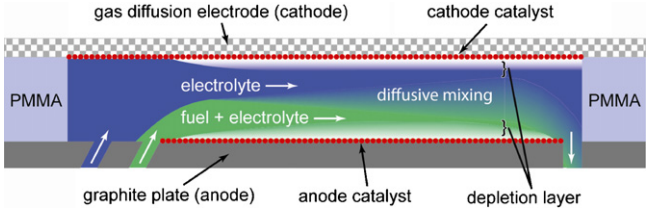

Fig. 1. Schematic of an air-breathing laminar flow-based fuel cell (LFFC): a 0.2-cm thick PMMA window is positioned between a catalyst-covered graphite plate (anode) and an air-breathing gas diffusion electrode (cathode).

electrodes and detailed characterization of performance-limiting factors [13].

This paper reports on the performance of air-breathing LFFCs operating with five different fuels (formic acid, methanol, ethanol, hydrazine, and sodium borohydride) in either acidic or alkaline media. In addition to demonstrating fuel and media flexibility, we present two powerful *in situ* analytical techniques, electrochemical impedance spectroscopy (EIS) and single electrode characterization, for investigating LFFC performance.

2. Experimental

2.1. Electrode preparation

For each fuel, unless noted otherwise, 10 mg/cm^2 of the appropriate noble metal catalyst and 1.5 mg/cm^2 of Nafion binder (DuPont) were painted onto an exposed area of the graphite plate used as an anode. For all experiments, unless noted otherwise, 2 mg/cm^2 unsupported platinum (Pt) nanoparticles (Alfa Aesar) and 0.1 mg/cm^2 Nafion binder were painted onto a Toray carbon paper gas diffusion layer (EFCG "S" type electrode, E-Tek). Table 1 shows the anode and cathode catalysts used with each fuel. After application of the catalyst ink, the cathode GDE was hot-pressed (Carver) at 340 psi and 130 °C for 5 min.

2.2. Fuel cell assembly and testing

A graphite plate (0.5-cm thick) with three holes (two inlets, and one outlet) was used as the anode. Polyethylene tubes (Cole Parmer, i.d. = 1.57 mm) were attached, with 5-min epoxy glue (Devcon, MA), to the inlets and outlet. A 0.2-cm thick polymethylmethacrylate (PMMA) separator with a precision machined 3-cm long, 0.33-cm wide window is placed directly over the anodic plate. The cathode GDE is positioned on top of the PMMA window with the catalyst facing the microfluidic channel. A graphite window functioning as a current collector is placed over the cathode. For the air-breathing configuration, a second PMMA sheet with a window is positioned over the current collector on the cathodic side to enable oxygen to diffuse from ambient air to the cathode. For the hydrogen cathode configuration, a polycarbonate chamber (5 cm (L) × 1 cm (W) × 0.5 cm (H)) was used to flow hydrogen (laboratory grade, S. J. Smith) over the cathode at 50 sccm. In both cases, the multilayer assembly was held together with binder clips (Highmark). Prior to experimentation, the LFFC was leak tested by flowing Millipore water through the fluidic chamber for several minutes. In the few cases leaking was observed, typically due to misalignment of the layers, the LFFC was disassembled and realigned. We did not observe leaking during subsequent operation of the LFFCs.

The fuel cell assembly was tested using acidic (anode stream: fuel + 0.5 M sulfuric acid (H_2SO_4), cathode stream: 0.5 M H_2SO_4) or alkaline (anode stream: fuel + 1 M potassium hydroxide (KOH), cathode stream: 1 M KOH) conditions. Fuel and electrolyte flow rates were controlled by a syringe pump (Harvard Apparatus). Unless noted otherwise, the flow rate of each of the streams was 0.3 mL/min (total flow rate of 0.6 mL/min). Polarization curves were obtained by steady-state chronoamperometric measurements at different cell potentials using a potentiostat (Autolab PGSTA-30, EcoChemie). Polarization curves were obtained by steady-state chronoamperometric measurements at different cell potentials using a potentiostat (Autolab PGSTA-30, EcoChemie). Potentiostat leads were attached to the anodic and cathodic graphite current collectors via copper alligator clips. The working electrode lead was attached to the anode while the reference and counter electrode leads were combined and attached to the cathode. The potentiostat was used to generate an applied potential, and a multimeter, with its leads attached to the anodic and cathodic graphite current collectors, was used to determine the actual cell potential. This configuration to measure the cell potential eliminates any contributions due to contact resistances between the alligator clips of the leads and the graphite current collector plates. The steady-state current measurements observed at each cell potential were recorded using General Purpose Electrochemical System (GPES) software (EcoChemie) provided with the potentiostat used. The exposed geometric surface area of the anode (0.66 cm^2) was used to calculate current and power densities. After passing between the anodic plate and the air-breathing cathode, the fluidic streams exit the fuel cell through a plastic tube (Cole Parmer, i.d. = 1.57 mm) and are collected in a beaker. A reference electrode (Ag/AgCl in saturated NaCl, BAS) was placed in the beaker enabling independent analysis of individual electrode polarization [11,13,14]. In prior work, we have shown that no significant potential drop occurs along the tubing connecting the fuel cell with the reference electrode [13]. Individual anode and cathode polarization was measured using two multimeters, functioning in voltmeter mode, attached to the reference electrode and each of the graphite plate current collectors. For the *in situ* single electrode characterization experiments and the electrochemical impedance spectroscopy (EIS) experiments (Autolab PGSTA-30 with FRA module, EcoChemie), a dynamic hydrogen electrode (DHE) was created by flowing hydrogen over the cathode. *In situ* single electrode studies were performed using the DHE as a counter and a reference electrode. Steady-state currents were recorded at different cell potentials using a potentiostat (Autolab PGSTA-30, EcoChemie). AC impedance spectra were measured in the constant voltage mode by decreasing frequencies from 10 kHz

Table 1
Fuels, electrode catalyst and total catalyst loading (mg/cm^2) combinations employed in all LFFC studies.

Fuel	Anode		Cathode	
	Catalyst	Loading (mg/cm^2)	Catalyst	Loading (mg/cm^2)
Formic acid	Pd black	10	Pt black	2
Methanol	Pt/Ru black	10	Pt black	2
Ethanol	Pt/Ru black	10	Pt black	2
Sodium borohydride	Pt black	10	Pt black	2
Hydrazine	Pt black	10	Pt black	2
	Pt/C	2	Pt/C	2

Pt/Ru black is 50:50 at.%, Pt/C is 50 wt% Pt on Vulcan XC 72R.

to 30 mHz at 9 points/decade. The modulating voltage was 10 mV root mean squared. The impedance spectra were used to measure internal cell resistance (R_{cell}) which includes electrolyte ionic conductivity and to measure charge-transfer resistance (R_{ct}) for the anodic fuel oxidation reactions. All studies were performed at room temperature.

2.3. Ex situ electrochemical studies

Single electrode studies of the individual anodes were performed in a three-electrode electrochemical cell. Pt wire (Alfa Aesar) and Ag/AgCl (BAS) were used as the counter and reference electrodes. Prior to testing, the fuel and electrolyte solutions were bubbled with nitrogen or argon to remove oxygen. Experiments were performed under a nitrogen or argon environment at room temperature. The steady-state currents were recorded at different cell potentials, using a potentiostat (Autolab PGSTA-30, EcoChemie), and compared to the *in situ* single electrode studies.

3. Results and discussion

Here, fuel and media flexible air-breathing laminar flow-based fuel cells (LFFCs) are investigated using five different fuels (formic acid, methanol, ethanol, hydrazine and sodium borohydride) under acidic or alkaline conditions. Furthermore, the same cell was used to demonstrate two easily-applicable *in situ* analytical techniques for anode optimization in a direct ethanol LFFC in both acidic and alkaline media.

3.1. Performance in acidic media

The performance of air-breathing LFFCs using methanol, ethanol, formic acid and hydrazine were investigated under acidic conditions (0.5 M H_2SO_4). The fifth fuel, sodium borohydride, is only studied in alkaline conditions (see below) because it is unstable under acidic conditions [15–17].

In Fig. 2a we show the cell performance for a LFFC operated with methanol (Pt/Ru anode catalyst, as reported previously [14]), as well as of LFFCs operated with ethanol (Pt/Ru anode catalyst) and formic acid (Pd anode catalyst). Peak power densities of 11.8, 1.90 and 26.0 mW/cm^2 and open circuit potentials (OCPs) of 0.93, 0.41 and 0.94 V were observed for methanol, ethanol and formic acid, respectively. The high OCP observed for the direct methanol LFFC compares favorably to OCPs of 0.5–0.8 V reported for Nafion-based DMFCs [4,18,19]. The higher OCP in the LFFCs studied here indicates minimal fuel crossover under the operating conditions used. Furthermore, the observed peak power density of 11.8 mW/cm^2 for the direct methanol LFFC is comparable to power densities reported for miniaturized conventional DMFCs of 2–15 mW/cm^2 [4,18,19]. The low performance of direct methanol and ethanol LFFCs, compared to the direct formic acid LFFC, can be attributed to poor oxidation kinetics in acidic media as evident from the anode polarization curves (Fig. 2b). Cathodic potential losses can be attributed to oxygen reduction reaction (ORR) overpotentials which can account for up to 0.3–0.4 V losses on Pt catalysts [20,21]. Both methanol and ethanol electro-oxidation are challenging multi-step reactions involving the formation of strongly adsorbed intermediate species on the catalytic surface [14,22,23]. Methanol oxidation is hindered by generated carbon monoxide (CO) which poisons the Pt/Ru catalyst surface reducing the electrochemically active surface area and exhibiting activation and kinetic losses. Similarly, ethanol oxidation is inhibited by generated CO and various C1 and C2 hydrocarbon residues which deactivate the Pt/Ru catalytic surface even worse. Complete ethanol electro-oxidation on Pt/Ru catalyst remains difficult as cleavage of the strong C–C bond is challenging [23,24].

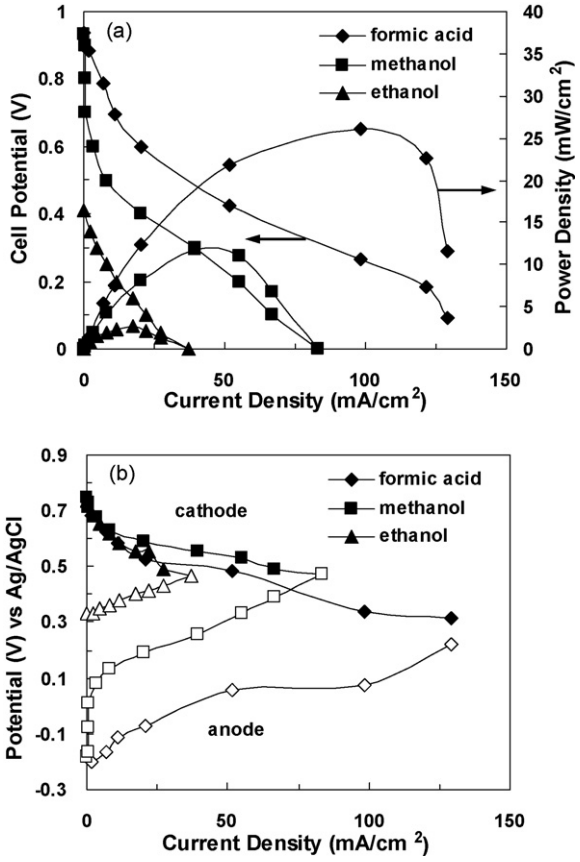

Fig. 2. (a) Polarization and power density curves of an air-breathing acidic LFFC operated formic acid, methanol and ethanol. (b) Corresponding anode and cathode polarization curves. In all experiments, [fuel] is 1 M, [H_2SO_4] is 0.5 M, stream flow rates were 0.3 mL/min and all testing was performed at room temperature.

These intermediates are removed via further oxidation by surface-adsorbed hydroxyls (OH), ideally to form carbon dioxide (CO_2). In acidic media, OH species are formed by the decomposition of water which occurs at high potentials leading to significant polarization losses on the anode [25]. Indeed, Pt/Sn alloys are known to exhibit enhanced ethanol oxidation activity compared to Pt/Ru, but C–C bond cleavage is still a problem [26,27]. The focus of this study is highlighting the fuel and media flexibility afforded to air-breathing LFFCs by the membraneless architecture, so we used Pt/Ru catalyst for both methanol and ethanol. The enhanced performance of direct formic acid LFFCs can be attributed to superior formic acid oxidation kinetics on the Pd catalyst used. Formic acid directly oxidizes to CO_2 on Pd catalyst bypassing the formation of CO intermediates resulting in acidic direct formic acid LFFCs to deliver the highest power densities [28]. Despite lower LFFC performances, both methanol and ethanol are still regarded as promising fuels due to their high energy densities, 6073 and 8028 Wh/g, respectively, compared to formic acid, 1630 Wh/g.

Direct hydrazine fuel cells are eco-friendly zero-emission power sources because hydrazine produces only protons and nitrogen gas upon complete electro-oxidation [29–32]. At low hydrazine concentrations (*i.e.* 1 M) in 0.5 M H_2SO_4, poorly soluble hydrazine sulfate is formed as evidenced by the appearance of a white precipitate. In contrast, at a hydrazine concentration of 3 M in 0.5 M H_2SO_4, more soluble dihydrazine sulfate forms [33]. Thus, we performed all experiments with 3 M hydrazine. The polarization and power density curves shown in Fig. 3a represent the performance of a direct hydrazine LFFC using unsupported catalyst (anode: 10 mg/cm^2 Pt and cathode: 2 mg/cm^2 Pt) and carbon-supported catalyst (anode

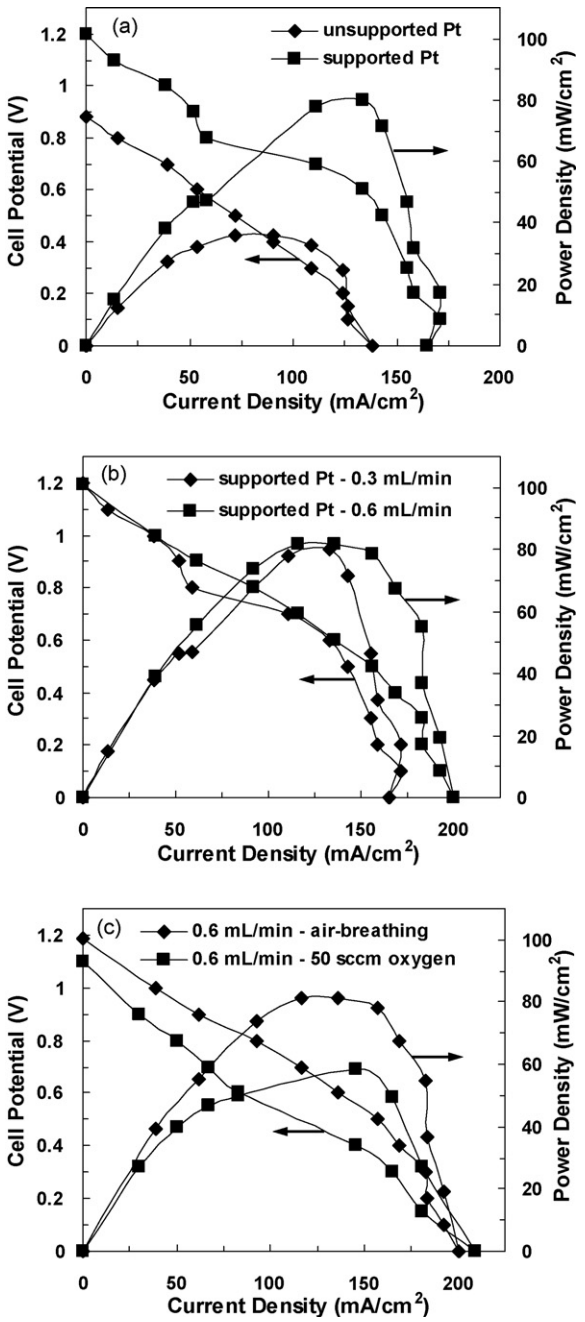

Fig. 3. (a) Polarization and power density curves of an air-breathing acidic LFFC operated with hydrazine using unsupported Pt catalysts (anode: 10 mg/cm^2 Pt and cathode: 2 mg/cm^2 Pt) and supported Pt catalysts (anode and cathode: 1 mg/cm^2 Pt). Further polarization and power density curves for LFFC operated with hydrazine and using supported Pt catalysts at (b) different flow rates and (c) with different oxygen delivery methods. In all experiments, [hydrazine] is 3 M and [H_2SO_4] is 0.5 M and all testing was performed at room temperature.

and cathode: 2 mg/cm^2 Pt on Vulcan XC-72R (Pt/C), 50 wt% Pt, E-Tek; *hitherto referred to as 1 mg/cm^2 Pt*). Peak power densities of 36.1 and 80.0 mW/cm^2 were observed when using unsupported and supported Pt catalyst, respectively. The dramatic improvement in cell performance using carbon-supported catalysts is due to (i) reduced particle aggregation which improves Pt utilization and (ii) minimized resistive losses in the catalyst layer due to the improved conductivity of the carbonaceous support. The maximum power density observed with the supported catalyst coincides with the onset of mass transport limitations. When the fuel and electrolyte stream flow rates are each increased from 0.3 to 0.6 mL/min, the peak power density remains constant while the maximum current density slightly increases (Fig. 3b). When the cathode was exposed to a 50 sccm oxygen flow rather than quiescent air, the peak power density and maximum current density did not increase (Fig. 3c), which indicates that this LFFC configuration, with supported Pt catalysts, is not limited by oxygen transport.

The performance of the direct hydrazine LFFCs reported here compares favorably to those reported in literature [29–31]. Direct hydrazine fuel cells reported in the literature use Nafion 117-based membrane electrode assemblies using 2 or 3 mg/cm^2 of unsupported Pt catalyst and operating at 80 °C with a forced oxygen flow on the cathode side [31]. These cells deliver a peak power density of 60 mW/cm^2 whereas the air-breathing, membraneless LFFCs reported here produce 80 mW/cm^2 at room temperature with a relatively lower Pt catalyst loading of 1 mg/cm^2.

3.2. Performance in alkaline media

Next, the performances of air-breathing LFFCs using methanol, ethanol, and sodium borohydride as fuels were investigated under alkaline conditions (1 M KOH). The polarization and power density curves shown in Fig. 4a represent the cell performance with methanol and ethanol (both at 1 M). Peak power densities of 17.2 and 12.1 mW/cm^2 were observed for methanol and ethanol, respectively. The significant improvement in the performance of direct methanol and direct ethanol LFFCs are due to enhanced alcohol oxidation kinetics and oxygen reduction kinetics in alkaline media (Fig. 4b) compared to their performance in acidic media [34–36]. Furthermore, the higher open circuit potentials and improved performance indicate less electrode surface poisoning. Specifically, the

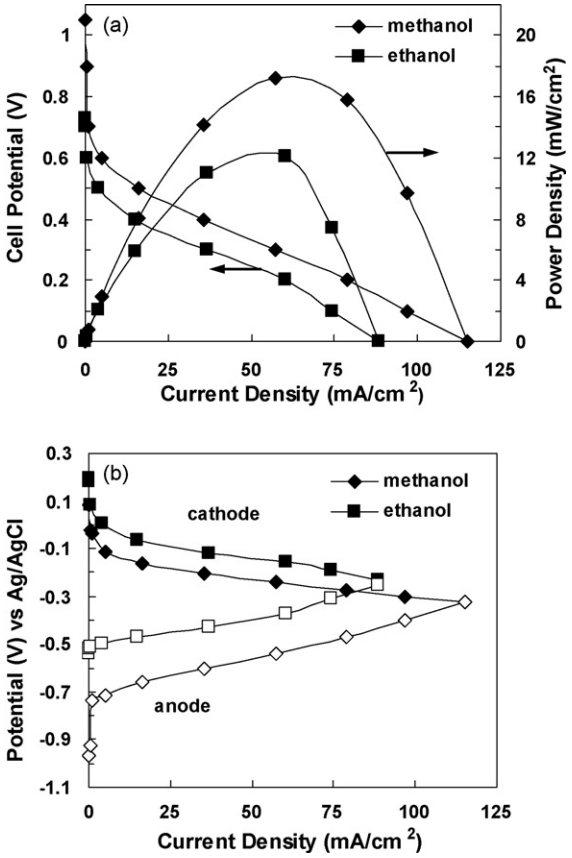

Fig. 4. (a) Polarization and power density curves of an air-breathing alkaline LFFC operated with methanol and ethanol. (b) Corresponding anode and cathode polarization curves. In all experiments, [fuel] is 1 M, [KOH] is 1 M, stream flow rate is 0.3 mL/min and all testing was performed at room temperature.

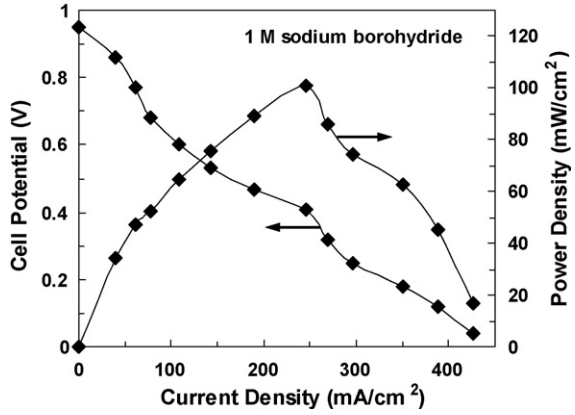

Fig. 5. Polarization and power density curves of an air-breathing alkaline LFFC operated with 1 M sodium borohydride and in 1 M KOH both flowing at 0.3 mL/min at room temperature.

strongly adsorbed intermediates formed at the anode, *i.e.* CO, C1 and C2 hydrocarbon residues, formed at the anode oxidize more readily by reacting with surface OH species which readily adsorb from the alkaline solution.

Sodium borohydride, the fifth fuel studied, has an energy density of 9295 Wh/g, is often discounted as a fuel due to its limited stability in acidic media [15–17]. However, sodium borohydride is highly stable in alkaline media [37]. Moreover, LFFCs can operate interchangeably in acidic or alkaline media thus direct borohydride LFFCs hold promise as a micro-scale power source [9,14,38]. The polarization and power density curves (Fig. 5) represent the LFFC performance using a 1 M sodium borohydride and 1 M KOH where a peak power density of 101 mW/cm^2 was observed. This excellent performance is due to the enhanced electrocatalytic activity of Pt towards the oxidation of the borohydride anion as compared to the other fuels studied here.

3.3. *In situ* diagnostics

In addition to facilitating fuel and electrolyte flexibility, the membraneless LFFC architecture enables the *in situ* application of two powerful analytical techniques: single electrode characterization and electrochemical impedance spectroscopy (EIS). A dynamic hydrogen electrode (DHE) is created by flowing hydrogen over the cathode. This cathode now serves as both the reference and counter electrode and thus provides a simple and accurate means of anode characterization within an operating fuel cell. Such a characterization platform is ideal for elucidating electrode kinetics and transport processes that govern anode performance. Previously, others have used a hydrogen cathode to investigate anode performance in DMFCs [39–41]. However, as with all polymer electrolyte membrane-based fuel cell systems, the electrode analysis is hampered by membrane limitations such as water management. A laminar flow-based characterization platform not only eliminates these membrane-related constraints but also enables operation under wide range of experimental conditions, *i.e.* adjustable pH within a single cell. The performance of DE-LFFC under acidic (0.5 M H_2SO_4) and alkaline (1 M KOH) conditions can be compared as the DHE shifts linearly with pH, approximately −59 mV per pH unit [36].

The two diagnostic methods are demonstrated using a direct ethanol LFFC (DE-LFFC) in alkaline or acidic media, and operated with a hydrogen cathode as explained above. As previously mentioned, ethanol is a promising fuel due to its high energy density and its availability from biomass [15]. Poor ethanol electro-oxidation kinetics are a key obstacle in the development of direct ethanol fuel cells. For both diagnostic methods, carbon paper with the desired anode catalyst loading is clamped between the graphite plate and the microfluidic channel. Three holes in the carbon paper provide access for the two inlet streams and the one outlet stream. Now *in situ* (LFFC) and *ex situ* (3-electrode cell) electrode performance data can be directly compared. In the 3-electrode cell, the linear potential offset due to the pH difference between the acidic and alkaline media was accounted for by comparing data on a stationary absolute scale, versus a reversible hydrogen electrode (RHE) as we have shown previously [14,36]. Fig. 6a shows single electrode studies characterizing anode performance in acidic and alkaline media in a 3-electrode cell. At potentials greater than 0.65 V vs. RHE, the anode, in both media, encounters mass transport limitations (data not shown). *In situ* single electrode studies, in the LFFC (Fig. 6b) show similar trends which confirms appropriate performance of the LFFC-based analytical platform. As previously mentioned, for the *in situ* measurements, the hydrogen cathode acts as the DHE and provides a stationary absolute scale for comparing acidic and alkaline data. Note, the extent of mass transport is a key difference between the studies. Unlike the 3-electrode cell which relies on diffusive transport, the LFFC relies on convective transport thus no mass transport limitations are observed at potentials greater than 0.65 V vs. DHE. The flowing fuel and electrolyte streams simultaneously decrease the depletion boundary layer thickness and increase the driving force of ethanol transport to the anode. For both the 3-electrode and the LFFC-based cells, ethanol oxidation in alkaline media starts at a lower potential and produces higher current densities than in acidic media due to the aforementioned enhanced reaction kinetics in alkaline solution [34,36].

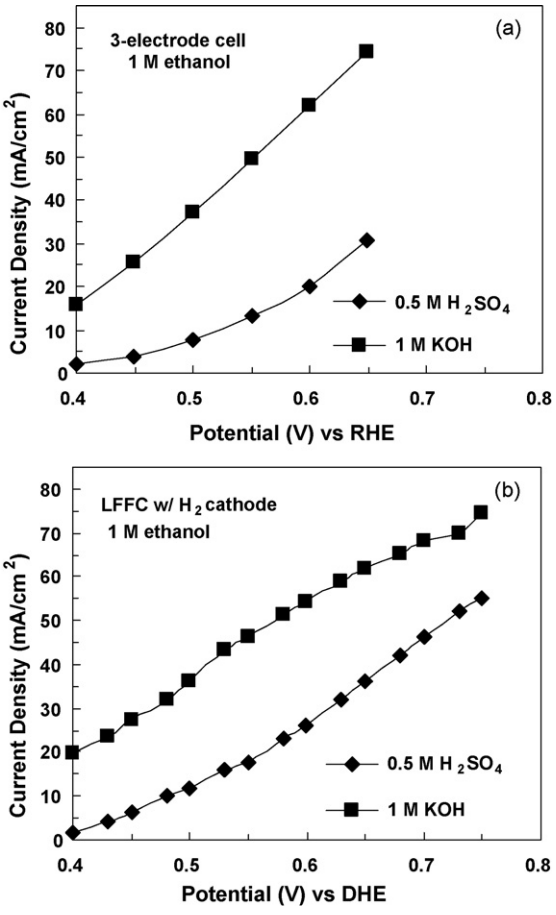

Fig. 6. Single electrode characterization of a DE-LFFC anode in (a) a three-electrode cell, and in (b) a LFFC using a hydrogen cathode. In all experiments, [ethanol] is 1 M, [H_2SO_4] is 0.5 M, [KOH] is 1 M, stream flow rates are 0.3 mL/min (in the LFFC) and all testing was performed at room temperature.

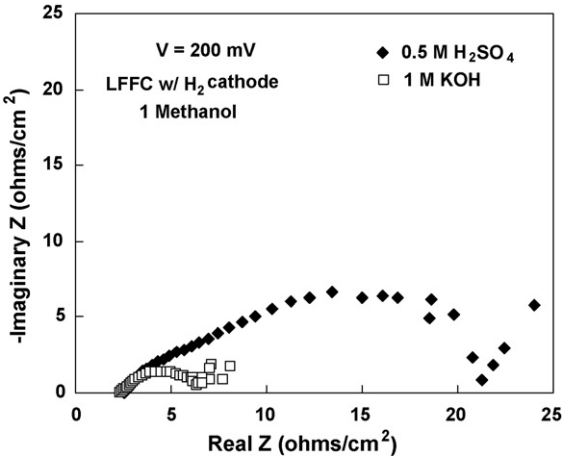

Fig. 7. Impedance spectra of DE-LFFC operated with 1 M ethanol under both acidic (0.5 M H_2SO_4) and alkaline (1 M KOH) conditions at stream flow rates of 0.3 mL/min. A hydrogen cathode was used as a counter/reference electrode and the cell potential is 200 mV.

We further characterized the performance of a DE-LFFC operated in either acidic (0.5 M H_2SO_4) or alkaline (1 M KOH) media using electrochemical impedance spectroscopy (EIS). For these experiments, a hydrogen cathode was used instead of an air-breathing cathode. This will minimize the cathodic contribution to the overall fuel cell response because the hydrogen evolution reaction kinetics are significantly faster than ORR kinetics [42]. In EIS studies, a small alternating current perturbation of varying frequency is applied to a DE-LFFC to decouple the transport and electrochemical phenomena that govern fuel cell performance. In Fig. 7, the Nyquist plots of both experiments exhibit similar features that only differ in magnitude. The high frequency intercept (initial data point closest to the original) on the *x*-axis represents the cell resistance (R_{cell}), which includes electrolyte solution resistance and any contact resistances. Here, the observed R_{cell} values are 2.5 and 2.4 Ω/cm^2 for the fuel cell configuration operated with acidic and alkaline media, respectively. The difference between these measured resistances and the solution resistance (0.85 and 0.92 Ω for 0.5 M H_2SO_4 and 1 M KOH, respectively [43]) is due to contact resistance between the alligator clips and the graphite current collectors on the order of 1.5 Ω/cm^2. Comparative analyses can still be performed because the exact same fuel cell configuration is used in both cases.

The semicircular-shaped curves represent the electrode reactions, which can be described by two R_{ct}–C_{cpe} parallel circuits with different time constants. C_{cpe} is a constant phase element capacitance describing the porous, distributed nature of the GDEs [44]. R_{ct} is the charge-transfer resistance, with the diameter of the semicircular-shaped curves representing the combined R_{ct}'s of the anodic and cathodic electrochemical reactions. Here, the measured R_{ct} values are 18.8 and 4.2 Ω/cm^2 for the fuel cell configuration operated with acidic and alkaline media, respectively. The lower R_{ct} observed under alkaline conditions is further evidence of more facile ethanol oxidation reaction kinetics in alkaline media confirming the results observed in the *in situ* single electrode studies (Fig. 6) and the DE-LFFC performance studies (Figs. 2 and 4).

At high frequencies, a discernable inflection exists in the semicircular features of both Nyquist plots, indicative of multiple contributions to the overall charge-transfer resistance. The slow ethanol oxidation reaction on the anode is the dominant contribution. Ion resistance and transport limitations within the porous GDEs are known as possible additional contributions causing an inflection [44,45].

At low frequencies, a "Warburg" response (approximately linear continuation of the data, at a 45° angle) is observed under both operating conditions. This indicates that mass transport, specifically ethanol diffusion to the anode, is limiting DE-LFFC performance [46]. Such mass transport limitations are expected considering the low cell potential of 0.2 V (*i.e.* high current densities) at which these EIS spectra were obtained. This comparative analysis confirms that enhanced reaction kinetics is the source of the observed performance improvements for DE-LFFCs operated with alkaline media.

Furthermore, the above also highlights that use of a hydrogen electrode as the cathode allows for detailed *in situ* anode studies. The anode environment can be tailored by controlling composition of the fuel and electrolyte streams. Thus, the present fuel cell configuration has potential as an analytical platform to investigate and optimize novel catalysts, electrode architectures as well as protocols for their preparation.

4. Conclusions

The membraneless architecture of laminar flow-based fuel cells (LFFCs) not only facilitates fuel and electrolyte flexibility but enables the simple *in situ* application of powerful analytical methods. Here, we demonstrate the versatility of air-breathing LFFCs using a wide range of liquid fuels (methanol, ethanol, formic acid, hydrazine and sodium borohydride) under acidic and alkaline conditions. Acidic LFFCs operated with formic acid showed superior performance as compared to methanol and ethanol however both alcohols remain promising fuels due to their high energy densities. A hydrazine fueled acidic LFFC compares very favorably with results reported in literature and appears a promising micro-scale power source for applications where safety is less of an issue than, for example, in consumer electronics. Enhanced electro-activity was observed for alkaline LFFCs. As long as the fuel is stable in alkaline media, as is the case for methanol, ethanol and sodium borohydride, but not for hydrazine and formic acid, this advantage of enhanced performance can be exploited when using a LFFC.

In the various LFFC experiments with different fuels, anode catalysts are matched to the fuel to optimize electro-oxidation kinetics. Because some fuels use identical catalysts, *e.g.*, methanol and ethanol use Pt/Ru, hydrazine and sodium borohydride use Pt, such LFFCs may be interchangeably operated with a desired and/or available fuel and media combination. The performance of the air-breathing LFFCs operating with the different fuels reported here may still be further optimized by varying structural parameters (*e.g.*, electrode-to-electrode distance, electrode length) and/or operational parameters (*e.g.*, higher flow rates, higher temperature, electrolyte composition). In addition, better electrical connections will significantly reduce the contact resistances encountered in some of the experiments. Moreover, the catalyst composition (*e.g.*, Pt/Sn as opposed to Pt/Ru catalyst for DE-LFFCs) and electrode preparation procedures can be optimized further.

The introduction of a hydrogen cathode transformed the air-breathing LFFC into a robust fuel and media flexible anode characterization platform. This configuration enables optimization of anode performance using *in situ* single electrode characterization and EIS to elucidate reaction kinetics and to identify performance limiting factors. This tool is particularly useful for investigating challenging reactions, *i.e.* ethanol electro-oxidation. Furthermore, this platform enables rapid and inexpensive testing of novel catalysts and electrode architectures in an operating fuel cell under a wide range of experimental conditions. However, any optimization effort also must keep overall fuel cell system implications in mind because varying any operational parameter will not only impact power density but also fuel utilization [12].

Acknowledgements

We gratefully acknowledge financial support from the National Science Foundation (Career Grant CTS 05-47617), the Department of Energy (Grant DEFG02005ER46260), Northrop Grumman, and a Graduate Engineering for Minorities (GEM) Fellowship for F.R. Brushett. Furthermore, the authors thank M.S. Naughton and J.D. Tice for stimulating discussions.

References

[1] L. Carrette, K.A. Friedrich, U. Stimming, ChemPhysChem 1 (2000) 162.
[2] A. Kundu, J.H. Jang, J.H. Gil, C.R. Jung, H.R. Lee, S.H. Kim, B. Ku, Y.S. Oh, J. Power Sources 170 (2007) 67.
[3] G.J.K. Acres, J. Power Sources 100 (2001) 60.
[4] S.C. Kelley, G.A. Deluga, W.H. Smyrl, Electrochem. Solid State Lett. 3 (2000) 407.
[5] C. Rice, R.I. Ha, R.I. Masel, P. Waszczuk, A. Wieckowski, T. Barnard, J. Power Sources 111 (2002) 83.
[6] L.A. Adams, S.D. Poynton, C. Tamain, R.C.T. Slade, J.R. Varcoe, ChemSusChem 1 (2008) 79.
[7] J.R. Varcoe, R.C.T. Slade, E. Lam How Yee, Chem. Commun. (2006) 1428.
[8] J.R. Varcoe, R.C.T. Slade, Fuel Cells 5 (2005) 187.
[9] E.R. Choban, L.J. Markoski, A. Wieckowski, P.J.A. Kenis, J. Power Sources 128 (2004) 54.
[10] L.J. Markoski, P.J.A. Kenis, E.R. Choban, Fuel cells comprising laminar flow induced dynamic conducting interfaces, USA 2004072047 (2004).
[11] R.S. Jayashree, L. Gancs, E.R. Choban, A. Primak, D. Natarajan, L.J. Markoski, P.J.A. Kenis, J. Am. Chem. Soc. 127 (2005) 16758.
[12] R.S. Jayashree, S.K. Yoon, F.R. Brushett, D. Natarajan, L.J. Markoski, P.J.A Kenis, unpublished results.
[13] E.R. Choban, P. Waszczuk, P.J.A. Kenis, Electrochem Solid State Lett. 8 (2005) A348.
[14] R.S. Jayashree, D. Egas, J.S. Spendelow, D. Natarajan, L.J. Markoski, P.J.A. Kenis, Electrochem. Solid State Lett. 9 (2006) A252.
[15] U.B. Demirci, J. Power Sources 169 (2007) 239.
[16] C.P. de Leon, F.C. Walsh, D. Pletcher, D.J. Browning, J.B. Lakeman, J. Power Sources 155 (2006) 172.
[17] J.H. Wee, J. Power Sources 161 (2006) 1.
[18] T. Shimizu, T. Momma, M. Mohamedi, T. Osaka, S. Sarangapani, J. Power Sources 137 (2004) 277.
[19] T.J. Yen, N. Fang, X. Zhang, G.Q. Lu, C.Y. Wang, Appl. Phys. Lett. 83 (2003) 4056.
[20] H.A. Gasteiger, S.S. Kocha, B. Sompalli, F.T. Wagner, Appl. Catal. B-Environ. 56 (2005).
[21] J.K. Norskov, J. Rossmeisl, A. Logadottir, L. Lindqvist, J.R. Kitchin, T. Bligaard, H. Jonsson, J. Phys. Chem. B 108 (2004) 17886.
[22] J.S. Spendelow, G.Q. Lu, P.J.A. Kenis, A. Wieckowski, J. Electroanal. Chem. 568 (2004) 215.
[23] C. Lamy, A. Lima, V. LeRhun, F. Delime, C. Coutanceau, J.M. Leger, J. Power Sources 105 (2002) 283.
[24] S. Rousseau, C. Coutanceau, C. Lamy, J.M. Leger, J. Power Sources 158 (2006) 18.
[25] H.S. Liu, C.J. Song, L. Zhang, J.J. Zhang, H.J. Wang, D.P. Wilkinson, J. Power Sources 155 (2006) 95.
[26] E. Antolini, J. Power Sources 170 (2007) 1.
[27] P.E. Tsiakaras, J. Power Sources 171 (2007) 107.
[28] Y.M. Zhu, Z. Khan, R.I. Masel, J. Power Sources 139 (2005) 15.
[29] K. Yamada, K. Yasuda, H. Tanaka, Y. Miyazaki, T. Kobayashi, J. Power Sources 122 (2003) 132.
[30] K. Yamada, K. Yasuda, N. Fujiwara, Z. Siroma, H. Tanaka, Y. Miyazaki, T. Kobayashi, Electrochem. Commun. 5 (2003) 892.
[31] K. Yamada, K. Asazawa, K. Yasuda, T. Ioroi, H. Tanaka, Y. Miyazaki, T. Kobayashi, J. Power Sources 115 (2003) 236.
[32] K. Asazawa, K. Yamada, H. Tanaka, A. Oka, M. Taniguchi, T. Kobayashi, Angew. Chem. Int. Edit. 46 (2007) 8024.
[33] R.C. Weast, Handbook of Chemistry and Physics, The Chemical Rubber Co, Cleveland, 1968, p. B-203.
[34] A.V. Tripkovic, K.D. Popovic, B.N. Grgur, B. Blizanac, P.N. Ross, N.M. Markovic, Electrochim. Acta 47 (2002) 3707.
[35] A.V. Tripkovic, K.D. Popovic, J.D. Lovic, V.M. Jovanovic, A. Kowal, J. Electroanal. Chem. 572 (2004) 119.
[36] J.S. Spendelow, A. Wieckowski, Phys. Chem. Chem. Phys. 9 (2007) 2654.
[37] M.I. Bellavance, B. Miller, Encyclopedia of Electrochemistry of the Elements, Marcel Dekker, 1974.
[38] E.R. Choban, J.S. Spendelow, L. Gancs, A. Wieckowski, P.J.A. Kenis, Electrochim. Acta 50 (2005) 5390.
[39] M. Baldauf, W. Preidel, J. Appl. Electrochem. (2001) 781.
[40] S.C. Thomas, X.M. Ren, S. Gottesfeld, P. Zelenay, Electrochim. Acta 47. (2002).
[41] R.Z. Jiang, D.R. Chu, J. Electrochem. Soc. 151 (2004).
[42] S. Srinivasan, Fuel Cells: From Fundamentals to Applications, Springer Science+Business Media, New York, 2006.
[43] G. Prentice, Electrochemical Engineering Principles, Prentice Hall, Englewood Cliffs, 1991.
[44] J.R. Varcoe, R.C.T. Slade, G.L. Wright, Y.L. Chen, J. Phys. Chem. B 110 (2006).
[45] T.J.P. Freire, E.R. Gonzalez, J. Electroanal. Chem. 503 (2001).
[46] A.J. Bard, L.R. Faulkner, Electrochemical Methods: Fundamentals and Applications, 2nd ed., John Wiley & Sons, Hoboken, 2001.